

Polymerization-Induced Wrinkled Surfaces with Controlled Topography as Slippery Surfaces for Colorado Potato Beetles

Johannes B. Bergmann, Dafni Moatsou,* Venkata A. Surapaneni, Marc Thielen, Thomas Speck, Bodo D. Wilts,* and Ullrich Steiner*

Controlling the interaction of insect populations with their host plants has recently received renewed attention in the light of pest control. One way to modify the interaction of insects with their host plants in a non-chemical way is through influence of their de/attachment. Insect detachment has been observed for textured biological and structured artificial surfaces with morphologies ranging from nano- to micrometers (0.3–1.5 μm). Here, the formation of design surfaces is investigated through plasma-induced polymerization of acrylates. This produces pronounced surface wrinkles that are tunable by the manufacturing process. For certain parameters, the wrinkles resemble those of the adaxial side of rubber tree (*Hevea brasiliensis*) leaves, a natural example of particularly low friction. Traction force measurements on the bio-inspired surfaces show significantly impacted insect attachment compared to flat surfaces of silica and polymeric materials, opening a pathway to the controlled manufacture of bio-inspired slippery surfaces for insects that could potentially find use in advanced materials such as wall coatings.

structures with minimized adhesion properties are the leaves of the sacred lotus (*Nelumbo nucifera*), whose remarkable hierarchical surface properties have been extensively studied and transferred to synthetic biomimetic materials.^[5,6] The lotus is not the only plant with superhydrophobic (water contact angles $>150^\circ$) leaves based on a combination of surface topography and/or a hydrophobic chemistry. Wrinkled, nanostructured surfaces have indeed evolved multiple times across the natural kingdom and can be found in a plethora of forms, ranging from “simple” wrinkled surfaces on leaves, such as the rubber tree *Hevea brasiliensis*,^[7] to more complicated folded, hierarchical materials found in several plant surfaces^[8–11] and grasshopper bronchosomes.^[4]


1. Introduction

The diverse, multifunctional surfaces of biological systems, such as those of plant leaves, flower petals, and animal integuments, may serve as inspiration to various technological applications and scientific research areas. Plant surfaces feature a vast array of functional adaptations with equally diverse properties, including the reduction of particle or insect adhesion as well as self-cleaning properties.^[1–4] Particularly interesting biological

Biomimetic research aims to mimic and transfer biological principles and functional structures to artificial technical materials and surfaces.^[12] Several methods have been reported to generate and manipulate ‘bio-inspired’ surface micro- and nanostructures, such as soft lithography, ion beam etching, and molding or stamping.^[13–15] 3D micro-rough structured surfaces exhibit ordered or semi-ordered structures with length scales spanning several orders of magnitude (from nm to macroscopic length scales).^[16] For the successful fabrication of micro-rough surfaces, it is important to control the pattern formation over

J. B. Bergmann, Dr. B. D. Wilts, Prof. U. Steiner
Adolphe Merkle Institute
University of Fribourg
Chemin des Verdiers 4, Fribourg 1700, Switzerland
E-mail: bodo.wilts@unifr.ch; ullrich.steiner@unifr.ch

Dr. D. Moatsou
Institute of Organic Chemistry
Karlsruhe Institute of Technology
Fritz-Haber-Weg 6, Karlsruhe 76131, Germany
E-mail: dafni.moatsou@kit.edu

 The ORCID identification number(s) for the author(s) of this article can be found under <https://doi.org/10.1002/admi.202000129>.

© 2020 The Authors. Published by WILEY-VCH Verlag GmbH & Co. KGaA, Weinheim. This is an open access article under the terms of the Creative Commons Attribution-NonCommercial License, which permits use, distribution and reproduction in any medium, provided the original work is properly cited and is not used for commercial purposes.

V. A. Surapaneni, Dr. M. Thielen, Prof. T. Speck
Plant Biomechanics Group
Botanic Garden
Faculty of Biology
University of Freiburg
Schänzlestrasse 1, Freiburg 79104, Germany

V. A. Surapaneni, Dr. M. Thielen, Prof. T. Speck
Freiburg Materials Research Center (FMF)
University of Freiburg
Stefan-Meier-Strasse 21, Freiburg 79104, Germany

Prof. T. Speck
Cluster of Excellence livMatS@ FIT- Freiburg Center for Interactive Materials and Bioinspired Technologies
University of Freiburg
Georges-Köhler-Allee 105, Freiburg 79110, Germany

DOI: 10.1002/admi.202000129

multiple length scales as well as the order/disorder of the features.^[17]

One particularly promising route to produce structured surfaces over a large area with controlled size distributions is plasma treatment of surfaces. One example is plasma polymerization, which was broadly used in the 1960s and 1970s as a method to form organic thin films,^[18] which enables the formation of polymeric materials under the influence of plasma.^[19] Other methods entail surface treatment of polymeric materials, such as poly(styrene) sheets in order to promote hierarchical structuring through skin growth.^[17] Another interesting approach was previously reported by Abate et al. in which they employed bifunctional monomers, such as diacrylates, to form wrinkled polymer films upon O₂ plasma exposure.^[20]

While other methods may require several steps for good control over the wrinkling morphology, plasma-induced polymerization offers a straightforward tool to reliably produce 3D-patterned surfaces in the form of nano- and micro-sized surface folds in a one step process over large areas.^[20] Wrinkling of thin films via instability under compressive stresses leads to micron and sub-micron patterning of the polymer and has been shown to be a promising method to fabricate surfaces with controllable topography.^[21] Plasma induces a mechanical and chemical gradient, resulting in an elastic buckling instability on the film surface that results in periodic wrinkling that can be characterized by its wavelength λ and amplitude A (Figure 1C).^[22–24]

In biological literature, surface topographies are often described through their arithmetic roughness R_a (mean deviation from a planar surface), which quantifies the deviations of the surface of a substrate compared to an ideal flat layer. While this parameter is universally used for general quality control,

it does not provide any information about the wavelength and is insensitive to small changes in profile, therefore characterizing topography through the wavelength λ and amplitude A of the corresponding morphologies is a more effective method.^[25] Wrinkled surface topographies have been shown to have a major effect on insect attachment.^[26,27] Indeed, pronounced reduction of insect attachment and walking friction forces has been observed for textured surfaces with surface roughness ranging from 0.3–3 μm .^[27,28] In a study on the surface properties of plant leaves, Prüm et al. showed that leaf surface topographies with asperity amplitudes of 0.5 μm and corresponding wavelength values of 0.5–1.5 μm feature a critical amplitude variation that effectively reduces insect attachment.^[7,11] Other properties, such as material hydrophobicity, naturally also contribute to a decreased insect attachment, but amplitude variations have been reported to be dominant over these other effects.^[29–31]

Here, we use plasma-induced polymerization to form artificial surfaces with controlled surface morphologies using mixtures of acrylate monomers. We show that the surfaces exhibited pronounced wrinkles, the amplitude, and wavelength of which can be adjusted by varying the initial monomer solution composition. These surfaces were both physically and chemically characterized, their surface structures were compared to those on the adaxial side of the leaves of the rubber tree (*Hevea brasiliensis*), a natural example providing especially low traction to male Colorado potato beetles. Traction force measurements showed significantly reduced insect attachment compared to flat surfaces of silica and the corresponding flat polymer surfaces, opening a pathway to the controlled manufacture of bio-inspired slip-surfaces for insects.

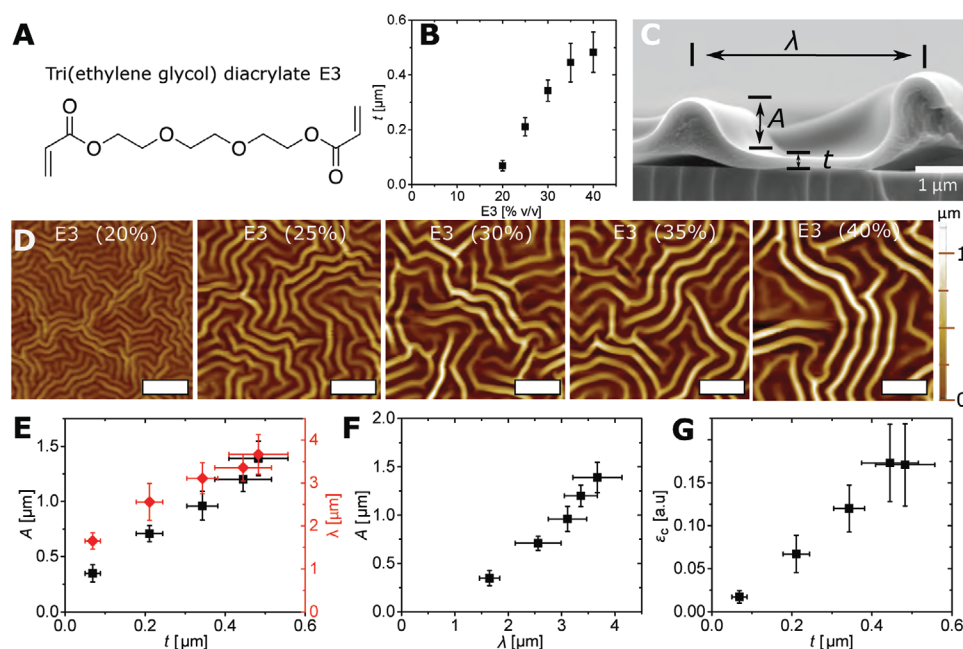


Figure 1. Plasma treatment of E3 solutions. A) Chemical structure of tri(ethylene glycol) diacrylate (E3). B) Film thickness t of polymerized E3 films as a function of monomer concentration. C) SEM image of a cross-section of a sample, showing two wrinkles and the extracted parameters: film thickness t , wrinkle amplitude A and wrinkle wavelength λ . D) AFM images of wrinkled thin films of E3 for solution concentrations varying from 20% v/v to 40% v/v. The scale bars represent 10 μm . E) Wrinkle amplitude and wrinkle wavelength of polymerized E3 films as a function of film thickness t . F) Wrinkle amplitude vs. wrinkle wavelength. G) Critical strain with respect to film thickness, according to Equation (1).

2. Results

2.1. Tri(ethylene Glycol) Diacrylate (E3) Polymer Films

E3 solutions in toluene with varying monomer concentrations c (20% v/v – 40% v/v) were prepared (Figure 1A). Films were spin-cast onto glass substrates yielding films of varying thicknesses, which were then exposed to an O_2 plasma. Since the thickness of the liquid film could not be reliably determined prior to the plasma treatment, the sample series is parametrized by the E3 solution concentration. Atomic force microscopy (AFM) was employed to characterize the surface wrinkling characteristics, that is, the wrinkle amplitude A , wavelength λ , and aspect ratio $AR = A/\lambda$. The film thicknesses t of the wrinkled polymer layers were determined by cross-sectional scanning electron microscopy (SEM) (Figure 1B,C).

At all investigated concentrations, the prepared polymer films featured distinctive surface wrinkling after plasma treatment (Figure 1C,D). The amplitude, wavelength, and the corresponding aspect ratio of the wrinkles varied across samples. With increasing concentration of E3 in the precursor solution, an increase in t , A and λ was observed (Figure 1B,E). The peak-to-peak λ -values ranged from $\lambda = 1.65 \pm 0.19 \mu\text{m}$ for $c = 20\% \text{ v/v}$ to $3.67 \pm 0.46 \mu\text{m}$ for $c = 40\% \text{ v/v}$, while the observed amplitudes A ranged from $0.35 \pm 0.08 \mu\text{m}$ for $c = 20\% \text{ v/v}$ to $1.39 \pm 0.16 \mu\text{m}$ for $c = 40\% \text{ v/v}$, monotonically increasing with increasing monomer concentrations. When comparing the amplitude A to the wrinkle wavelength λ , the aspect ratio AR increased slightly from 0.21 to 0.38 with increasing monomer concentration (Figure S1A, Supporting Information).

The critical strain ε_c quantifies the necessary compressive strain in order to induce out of plane deformations in the form of wrinkles.^[22] Elastic buckling theory relates the key parameters controlling surface wrinkling, via

$$\varepsilon_c = \pi^2 \frac{t^2}{\lambda^2} \quad (1)$$

The derivation of this equation is based on the buckling theory described in Equations (S1) and (S2), Supporting Information.^[22] Based on observation, ε_c increases linearly with increasing film thickness t , which is controlled by the monomer concentration (Figure 1G), varying from $\varepsilon_c = 0.017$, ($t = 70 \text{ nm}$, $c = 20\% \text{ v/v}$) to $\varepsilon_c = 0.173$ ($t = 445 \text{ nm}$, $c = 35\% \text{ v/v}$).

2.2. Controlling Crosslinking Density

So far, we have observed the thickness-dependence of the wrinkled surfaces for varying monomer concentrations. Another factor that influences wrinkling is the crosslinking density of the polymer materials. To investigate the impact of crosslinking density on the wrinkling properties of diacrylate thin films, we prepared precursor solutions with a total monomer concentration of 20% v/v in toluene, and varied the ratio of E3 to the corresponding monoacrylate G9. The monomer ratio f_{G9} is defined as the G9 volume fraction. The variation of the crosslinking density of polymerized G9/E3 mixtures was verified by measuring the glass transition temperature as a function of f_{G9} (Figure S3, Supporting Information).

AFM measurements of films with varying f_{G9} values are shown in Figure 2A, exhibiting an increased wrinkled surface area with decreasing f_{G9} values. For $f_{G9} > 0.72$, no distinct wrinkling patterns were microscopically observable, while for $f_{G9} < 0.72$, the wrinkle amplitude A increased linearly with decreasing f_{G9} . $f_{G9} \approx 0.7$ was identified as the “critical” monomer ratio, producing compressive surface strain values ε that exceeded the critical strain ε_c , thus leading to wrinkle

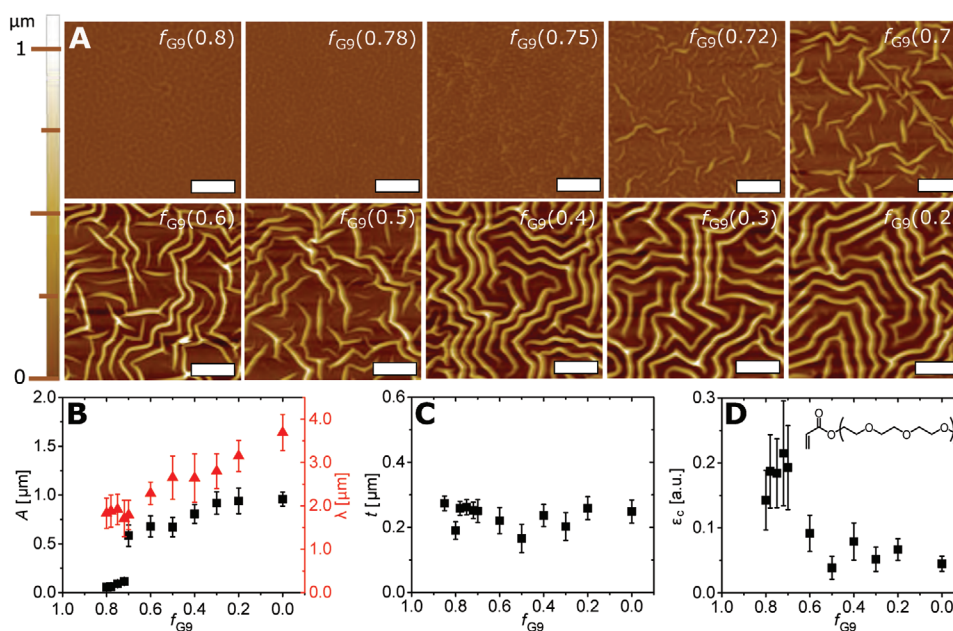


Figure 2. Plasma treatment of G9/E3 mixtures. A) AFM images of wrinkled thin films with varying G9/E3 mixing ratios. The scale bars are 10 μm . B) Wrinkle amplitude and wrinkle wavelength of polymerized films as a function of G9/E3 mixing ratio f_{G9} . C) Film thickness of produced wrinkled thin films versus f_{G9} . D) Critical strain ε_c versus f_{G9} , according to Equation (1). Inset: chemical structure of the G9 molecule.

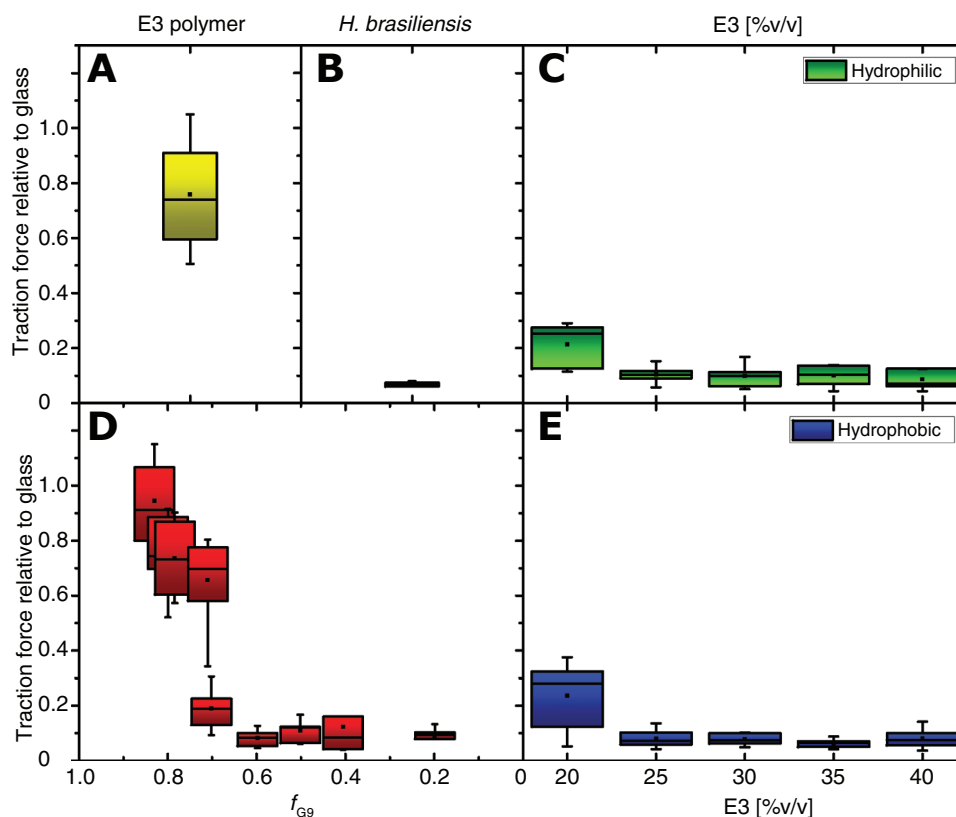


Figure 3. Traction force measurements. A) Traction force measurements of actively walking male potato beetles on a flat thermally-polymerized E3 surface and B) on the surface of a leaf of *Hevea brasiliensis*, relative to glass (from Prüm *et al.*^[11]). C) Traction forces on wrinkled surfaces, derived from varying E3 solution concentrations, relative to glass. D) Traction forces on wrinkled surface of films with varying f_{G9} ratios. E) Results of similar surfaces as in (C), after hydrophobization with trichloro(octyl)silane. ($N = 7$ for all measurements).

formation. The change in wrinkle amplitude from $f_{G9} = 0.72$ to $f_{G9} = 0.2$ was more than one order of magnitude, increasing from about 90 nm to over 958 nm. Note that the film thickness did not vary substantially with f_{G9} , in the 200–260 nm range (Figure 2C), as the overall monomer concentration (20% v/v) was kept constant. In order to keep the film thickness consistent, the spin-coating speed for the preparation of $f_{G9} = 0$ sample in Figure 2 was adjusted to 2000 rpm.

When comparing the mixed with the pure diacrylate system, the mixed system featured wrinkles with A and λ values that are comparable to the pure E3 system at concentrations between 25% v/v and 30% v/v (Figure 1E). The combined increase of λ and A resulted in nearly constant ARs in all films below the critical threshold, $f_{G9} < 0.70$, varying in the 0.28–0.34 range with a mean value of 0.29 ± 0.027 (Figure S1B, Supporting Information), comparable to the pure E3 system for a 20% v/v monomer concentration (Figure S1A, Supporting Information).

2.3. Traction Force Measurements

The effect of surface wrinkles on the attachment of beetles was assessed by comparing the prepared polymeric wrinkled surfaces to a biological system, namely the adaxial side of the leaves of the rubber tree, *Hevea brasiliensis*. Traction force measurements recorded the lateral forces of potato beetles, *Leptinotarsa*

dececlineata, walking on the prepared polymer samples (Figure 3), utilizing the setup previously reported by Prüm *et al.*^[7] Potato beetles are a well-established model species for this kind of studies, as they possess similar tarsal adhesive setae structures as typical pest insects feeding on *Hevea brasiliensis*. Male beetles were used as they have a well-described, more complex system of tarsal adhesive setae than female beetles^[11] and attach on glass surfaces better than females.^[27] We maintained this experimental protocol to make our data comparable to previous work. Typical magnitude of traction forces on glass surfaces ≈ 43.4 mN and on *Hevea brasiliensis* ≈ 1.8 mN were previously reported by Prüm *et al.*^[7] In the following, the measured traction forces were normalized to those measured on a glass surface (Equation (S3), Supporting Information).

The relative traction forces of male *L. dececlineata* (Figure 3) walking on wrinkled surfaces based on E3 and mixtures of E3 and G9 showed markedly decreased traction forces compared to that of a flat surface of thermally polymerized E3 (Figure 3A), which exhibited a slight reduction in traction force (compared to glass) of ≈ 0.75 . For the pure E3 system, the samples made with E3 concentrations between 25 and 40% v/v significantly reduced traction forces compared to a glass surface. For the lowest initial monomer concentration, 20% v/v ($A = 0.35$ μm ; $\lambda = 1.65$ μm), a relative mean traction force of ≈ 0.22 was measured (Figure 3C). Increasing monomer concentration and thus the wrinkle amplitude (c.f. Figure 1), further decreased the traction force to values

as low as 0.04 for $c = 35\%$ v/v ($A = 1.2 \mu\text{m}$; $\lambda = 3.36 \mu\text{m}$). To examine the influence of the surface polarity, as-prepared hydrophilic samples were compared to corresponding hydrophobic surfaces (hydrophobized by silane vapor deposition). No significant influence of the surface polarity on the attachment force was observed (Figure 3E). Comparing hydrophobic and hydrophilic wrinkled surfaces of the E3 system, the results show a very similar trend in terms of wrinkliness and resulting relative traction forces. Regardless of the polarity, a relative traction force reduction of up to 95% was observed.

The measured traction forces on wrinkled surfaces made from the G9/E3 blends (i.e., with changing crosslinking density) showed a similar reduction as the pure E3 system. Surfaces made with solutions above the critical ratio of $f_{G9} > 0.7$ (showing negligible wrinkling) exhibited traction properties comparable to glass. For wrinkled films made with $f_{G9} \leq 0.7$, the traction forces were comparable to the pure E3 films as well as the biological system (Figure 3B,D), with median values below 0.1. The reduced traction was clearly visible, with the beetles slipping when attempting to walk on these surfaces (Videos SV1–SV3, Supporting Information).

Since the reduction in traction forces of *L. decemlineata* is similarly efficient on the polymeric wrinkled surfaces compared to *Hevea brasiliensis* leaves, it is instructive to compare the structural parameters of both systems. The cuticular folds of *H. brasiliensis* leaves have amplitudes $A = 0.5 \mu\text{m}$ with varying wavelengths of $\lambda = 0.5\text{--}1.5 \mu\text{m}$ ($AR = 0.3\text{--}1$) resulting in relative traction forces as low as 0.04–0.02 (Figure 3B).^[31] For manufactured samples, comparably low relative traction values were found for amplitudes in the 0.7–1.4 μm range and wavelengths in the 2.5–3.5 μm range. When comparing the surface properties of the manufactured films and the adaxial side of the leaf of *H. brasiliensis*, we find different amplitudes (with $A_{\text{leaf}} < A_{\text{manufactured}}$) but comparable ARs. This indicates that the AR is the key parameter controlling insect attachment.

3. Discussion

The manufacture of bio-inspired wrinkled surfaces with controlled surface topologies by plasma treatment of commercially available acrylates is presented. The surface topography at the micrometer scale in the form of wrinkles can be controlled across one order of magnitude by varying the film thickness or the precursor composition which affects the crosslinking density of the films.

The formation of elastic wrinkles in hydrogels or other crosslinked composites has been observed before, albeit with different preparation methods. For example, Crosby et al. have shown that acrylate-based liquid films undergo self-wrinkling upon UV exposure.^[32] Rodriguez-Hernandez et al. have controlled the sub-micron morphology of such films through a combination of thermal and photo-crosslinking processes.^[33] Fery et al. have demonstrated photothermal as well as lithography-free methods for microstructuring surfaces through wrinkle induction.^[34,35] Wrinkling induced by plasma, as presented here, complements this work, enabling the tuning of the wrinkle parameters in a facile fashion. This technique can be readily applied to other monomers and crosslinking techniques, such as photo-polymerization.

Poly(ethylene glycol) (PEG)-based polymers are frequently employed in biomedical applications, particularly due to their excellent biocompatibility and tissue-like properties.^[36] The here employed acrylate PEG derivatives enable (photo-)polymerization due to the acrylate groups^[37] and the obtained crosslinked materials are reported to be non-toxic and biodegradable.^[38] Such diacrylates are commercially available in various molecular weights making them ideal to adapt and further optimize the presented system, for example, by tuning the crosslinking density (Figure 2). The tunable and non-toxic nature of crosslinked PEG diacrylate films make them an ideal candidate for attachment tests with living organisms and opens the door to possible real-life applications, such as anti-adhesive coatings for the food and agricultural sector.^[39]

3.1. Chemical Properties and Generalizability of The Manufacturing Approach

The formation of surface wrinkles requires a compressive stress in a surface layer (skin) on top of a compliant medium, described by elastic buckling. These systems are usually based on a rigid thin film connected to a flexible substrate with known properties. However, the formation of the skin layer in the present system is somewhat complex, since it involves a balance of both compressive and tensile stresses that are caused by the polymerization process. The plasma treatment induces polymerization at the surface of the liquid precursor films, causing the formation of a skin with a depth-dependent gradient in crosslinking density. The crosslinking of a polymeric material typically increases its density. On a substrate of lower crosslinking density (with the film edges anchored to the substrate), this causes a tensile stress within the film, which should stabilize the film against surface instabilities.^[40]

Mc Cormick et al. have described the physical properties of several curing systems following depth-dependent gradient curing, resolving this conundrum.^[41] The depth-dependent crosslinking of the monomers leads to a gradient in unreacted oligomers which in return causes the diffusion of unreacted or partially polymerized molecules into the skin, thereby swelling the skin. This swelling overcompensates the tensile stress caused by the initial crosslinking process and results in compressive stress in the edge-anchored skin. Surpassing a critical surface stress in the skin causes the formation of out-of-plane wrinkles. Further curing solidifies the remainder of the coating and fixes the wrinkle patterns. The final samples are fully cured (see Figure S2, Supporting Information).

In this model, the wrinkle pattern depends on a number of parameters, including the film thickness and the concentration of crosslinkable groups, both of which were varied in the experiments above. In the pure E3 system, wrinkling mechanics vary with film thickness, providing differing reservoirs for uncrosslinked monomers and thereby differing diffusion gradients during the plasma polymerization process. While these results can be qualitatively compared to elastic buckling equations, a quantitative model of this system is difficult due to the coupled nature of plasma-induced polymerization, the ensuing monomer diffusion and the gradual solidification of the film.

In the elastic buckling theory by Cerda and Mahadevan,^[21] A varies linearly with λ (Equation (S2), Supporting Information)

and additionally depends on the excess strain $\varepsilon - \varepsilon_c$. Wrinkling is only observed if $\varepsilon > \varepsilon_c$. This is qualitatively borne out by the monotonic variation of A with λ in Figure 1F. In this representation, the aspect ratio should vary weakly (as the square-root) with $\varepsilon - \varepsilon_c$. A comparison with the data (Figure S1A, Supporting Information) indicates a weak increase of $\varepsilon - \varepsilon_c$ with E3 solution concentration and thereby with the thickness of the liquid film prior to plasma treatment.

In standard buckling theories, where the stress in the skin is externally imposed, the critical strain depends exclusively on the ratio of plain-strain moduli of the skin versus the underlying medium, and is independent of geometrical parameters. When determining the critical strain ε_c from the data, in terms of Equation (1), a linear variation of the overall layer thickness t is found, clearly demonstrating that the kinetically evolving system described here is not quantitatively described by a simple buckling model.^[22]

While the control of wrinkling in the pure E3 system arises from variations of the layer thickness (controlled through the E3 solution concentration when spin-coating), the wrinkling properties in G9/E3 blends is controlled through the crosslinking density (Figure 2). E3, with two reactive groups forms a polymer network upon crosslinking, while G9 with only one reactive group reduces the density of crosslinks in the network. Varying crosslinking density through the G9/E3-ratio resulted in a change in both A and λ . For monomer ratios $f_{G9} \geq 0.72$, network formation seems to be too weak to cause wrinkling, which is observed only for $f_{G9} < 0.72$ (Figure 2B). Varying the crosslinking density causes changes in the gradient in unreacted monomers and therefore modulates the swelling of the skin that ultimately gives rise to the compressive stress that causes wrinkling.

While the solution film thickness (controlled through the monomer solution concentration) allows a variation of A and λ over a reasonably large range (i.e., by a factor of 10), changing the crosslinking density allows to fine-tune the buckling instabilities in these polymer thin films, in agreement with previous work on the mechanical response of amorphous polymers.^[42] Interestingly, in the experiments in which f_{G9} was changed, the aspect ratio and critical strain remained constant. Since in these films the film thickness was not varied, these two parameters are potentially primarily controlled by the overall layer thickness. In particular, the invariance of ε_c is surprising since according to simple buckling theories, this parameter is controlled by the skin/bulk modulus contrast, which should vary with crosslinking density.

To illustrate the versatility of our approach, these experiments were repeated with two further acrylates, as shown in Figure S4, Tables S1, and S2, Supporting Information. These results indicate that wrinkle formation can further be controlled by the nature of the utilized monomers, for example, the molecular weight of the reactants.

3.2. Beetle Attachment on Bio-Inspired, Wrinkled Surfaces

During coevolution with plants, insects developed two different attachment systems viz. hairy structures and smooth attachment pads on their legs as an adaptation to their habitats.^[43,44] The Colorado potato beetle, *Leptinotarsa decemlineata*, belongs to

the order Coleoptera, which have characteristic hairy attachment structures at their tarsi (tarsal adhesive setae).^[4,43] At the same time, plants developed different surface microstructures, like epicuticular waxes, cuticular folds, or trichomes, to deal with abiotic and biotic interactions including insects.^[45] Other insects (e.g. various beetle species) with similar hairy attachment structures as *L. decemlineata* were earlier shown to have preferential feeding behavior on *Hevea brasiliensis* leaves,^[46] possibly affected by the structural defence of the plant leaf surfaces.^[47] While the potato beetle is not a pest to *Hevea brasiliensis*, these beetles have immediate availability, are easy to experiment with, and serve as well-established model species possessing similar tarsal adhesive setae structures as typical pest insects feeding on *Hevea brasiliensis*. It is also interesting to note that the native habitat of these insects, the potato plants, do not appear to have cuticular structures similar to *Hevea brasiliensis*.

In accordance with several previous reports, the presented method of traction force measurement offers a good assessment of how the attachment of moving beetles are influenced by wrinkling of the substrate.^[11,31] The bio-inspired surfaces presented here cause traction force values generated by Colorado potato beetles that are comparable to the values obtained for the adaxial side of the leaf of the rubber plant (*Hevea brasiliensis*) and other biological surfaces (Figure 3).^[7] As postulated in these previous studies,^[26–28] it is the surface topography that significantly influences beetle attachment. Voigt et al.^[48] have previously investigated the effect of wrinkling anisotropy of PDMS-based surfaces on the attachment of beetles. While the wavelength of the wrinkles largely influenced the attachment of the beetles, their alignment seemed insignificant.

With surface topographies that are very similar to cuticular folds reported by Prüm et al., very similar insect attachment is found (Figure 3). Since the surface wettability (both hydrophilic and hydrophobic) of the manufactured surfaces were very different from the biological surface, this study confirms the hypotheses of the impact of both critical roughness as well as surface polarity onto beetle attachment. In particular, surface polarity is shown to have a negligible effect on insect attachment on wrinkled surfaces (Figure 3E).^[7] Clearly, for the reported values of surface wrinkles, the beetle attachment organs no longer have the ability to successfully attach to the surface.^[7] Our results suggest that the surface topography of the samples constitutes a contact splitting of the setae and therefore reduce the magnitude of the wet adhesion system as proposed by Federle et al.^[49]

In summary, we present a versatile platform for the preparation of wrinkled polymer films by plasma treatment of commercially available acrylates, allowing the design of surfaces with wrinkle topographies in the micrometer range. The influence of liquid film thickness (parameterized by the reagent concentration in the solution) and the crosslinking density in the polymer film (controlled by mixing two reagents) allowed the control over wrinkling parameters. For wrinkle parameters comparable to those of the rubber tree leaves (*Hevea brasiliensis*), the traction reduction in potato beetles walking on these surfaces was found to be indistinguishable for the biological and manufactured surfaces. This is unambiguous evidence that the surface wrinkles of both systems are effectively responsible for the reduction of

traction forces generated by Colorado potato beetles, by one order of magnitude relative to a glass reference. These results enable on the one hand even more careful studies of insect adhesion mechanisms, such as single-foot measurements as performed by Federle et al.^[50], and on the other hand may allow bio-inspired applications, particularly in the biomimetic design of green alternatives to chemical toxins in pest control in housing or crop protection.

4. Experimental Section

All chemicals were used as received, unless otherwise specified. Tri(ethylene glycol) diacrylate ($M_n \approx 250 \text{ g mol}^{-1}$, E3), poly(ethylene glycol) methyl ether acrylate ($M_n \approx 480 \text{ g mol}^{-1}$, G9), 1,6-hexanediol diacrylate (technical grade, 80%, M6) and trichloro(octyl)silane were obtained from Sigma-Aldrich. 1,10-Bis(acryloyloxy)decane, (M10) was purchased from ABCR. These acrylates were dissolved in toluene at solutions at concentrations ranging from 20% to 40% v/v. All solvents and other chemicals used were of analytical grade.

Plasma-Induced Polymerization: The acrylate-based films were prepared as follows: using a Laurell WS-400BZ spin coater, precursor solutions in toluene with monomer concentrations ranging from 20% to 40% (v/v) (total volume 400 μL) were spin-cast onto glass substrates (50 mm \times 50 mm). Spin coating was performed at 4000 rpm for 15 s at maximum acceleration. This resulted in a variation of the liquid film thickness which increased with acrylate solution concentration. Because of the low film viscosity and the tendency of the films to dewet, the thickness of the acrylate films could not be reliably measured. Upon spin-coating, the films were immediately transferred into a Plasma Etch PE-100-HF-RIE plasma etcher (40 kHz, 100 W max. power), in which plasma treatment was carried out. The procedure was as follows: The chamber was first evacuated and then flushed with O_2 for 2 min to remove any residual N_2 in the chamber's atmosphere. An activation energy of 50 W and a continuous gas flow rate of $3 \times 10^{-7} \text{ m}^3 \text{ s}^{-1}$ ($= 18 \text{ cc min}^{-1}$) of oxygen were employed.

Hydrophobization: Hydrophobization of the prepared wrinkled surfaces was done by vapor phase deposition (VPD) of trichloro(octyl)silane. The substrates were placed onto a sample holder in a desiccator, while 1 mL of trichloro(octyl)silane was placed in a Petri dish in the centre. The desiccator was closed and connected to a vacuum pump in order to maintain a static pressure of $\approx 0.4 \text{ mbar}$. An absorption trap was installed between the pump and the desiccator to avoid contamination. The samples were kept inside the desiccator for 20 min.

Imaging: The formation of wrinkles was imaged using a Zeiss Axio Scope A1 optical microscope in transmission mode. Images were taken with a Point Grey Grasshopper Camera. Scanning electron microscopy (SEM) images were obtained with a Tescan MIRA3 and a FEI Quanta 200 FEG scanning electron microscope. The plasma treated surfaces were first sputter-coated with a 4 nm gold layer employing a Cressington 208 HR (Cressington Scientific Instruments, Watford, UK) sputter coater to prevent charging. Cross-sectional images of wrinkles were obtained by fracturing the samples, which led to a partial delamination of the films.

Structural Characterization: A Park NX10 atomic force microscope (AFM) was used in intermittent contact mode (tapping) to characterize the topography of the wrinkled surfaces. Aluminum-coated silicon probes (NanoAndMore) with a nominal force constant of 40 N m^{-1} , a resonance frequency of 300 kHz, and a tip radius $< 10 \text{ nm}$ were employed. The water contact angle of the prepared surfaces was measured using an OSC 15Pro goniometer (DataPhysics Instruments, Filderstadt, Germany). 2 μL of water (deionized) were employed in all cases to ensure a consistent droplet size. The contact angle of the three-phase interface of the sessile drop was determined by fitting a tangent to the drop profile. Five measurements were conducted for each sample deriving the mean and standard deviation of the contact angles.

Thermal Characterization: Differential Scanning Calorimetry (DSC) analyses were performed using a Mettler-Toledo STAR under N_2 atmosphere. Samples of $\approx 7 \text{ mg}$ were heated from -20 to $100 \text{ }^\circ\text{C}$ and cooled back to $-20 \text{ }^\circ\text{C}$ at $10 \text{ }^\circ\text{C min}^{-1}$ for a total of three cycles. The glass transition temperature was determined through the derivative of the change in heat flow.

Insect Attachment; Male potato beetles, *Leptinotarsa decemlineata* (Say, 1824; Coleoptera: Chrysomelidae), were collected from organic potato fields in the Kirchzarten area near Freiburg, Germany (GPS coordinates: $47^\circ 57' 4'' \text{ N } 7^\circ 56' 5'' \text{ E}$), and kept in a terrarium on their host plant. The average weight of the employed beetles was $0.136 \pm 0.017 \text{ g}$ ($N = 7$).

For traction experiments, plasma treated samples were horizontally fixed to a table using double-sided adhesive tape. A force transducer (Fort 25, World Precision Instruments Inc., Sarasota, USA) was employed in order to measure the maximum traction forces of beetles while actively walking on the prepared samples. The force resolution was $\pm 50 \mu\text{N}$. Experiments were carried out at a steady temperature of $25 \text{ }^\circ\text{C}$ and a relative humidity of 35%. Each beetle was tethered to the force transducer using a wool thread (10 – 15 cm, average diameter = 0.231 mm ($N = 5$); Wenco Obergarn NE50/3), which was glued to the back of the beetle (elytra) with beeswax. The threads were fixed at the top and the mid region of the insect elytra. The traction forces were recorded with less than $\pm 2^\circ$ variation between the axis of the thread and sensing direction of the force transducer. In order to ensure active and straight walking, a small lamp was placed in front of the beetle to attract it. Measurements were stopped or not recorded if the beetle was not walking straight forward.

Supporting Information

Supporting Information is available from the Wiley Online Library or from the author.

Acknowledgements

The authors would like to thank Walter Federle for initial help and support. The authors also thank the brave potato beetles that endured the experiments. This work was financially supported by the European Commission through ITN "PlaMatSu" (722842), the Swiss National Science Foundation through an Ambizione grant (168223), the NCCR Bio-inspired Materials (51NF40-182881) and the Adolphe Merkle Foundation.

Author Contributions

J.B.B. and V.A.S. performed the experiments and analyzed the results. T.S. and U.S. conceived this study. D.M., M.T., B.D.W., and U.S. supervised the work. J.B.B., D.M., and B.D.W. wrote the first manuscript version and all authors edited the manuscript and approved final submission.

Conflict of Interest

The authors declare no conflict of interest.

Keywords

beetle adhesion, bio-inspired surfaces, plasma-induced polymerization, tunable surface properties

Received: January 24, 2020

Revised: March 17, 2020

Published online:

- [1] E. Gorb, K. Haas, A. Henrich, S. Enders, N. Barbakadze, S. Gorb, *J. Exp. Biol.* **2005**, *208*, 4651.
- [2] C. Neinhuis, W. Barthlott, *Ann. Bot.* **1997**, *79*, 667.
- [3] L.-q. Ren, S.-j. Wang, X.-m. Tian, Z.-w. Han, L.-n. Yan, Z.-m. Qiu, *J. Bionic Eng.* **2007**, *4*, 33.
- [4] T. B. H. Schroeder, J. Houghtaling, B. D. Wilts, M. Mayer, *Adv. Mater.* **2018**, *30*, 1705322.
- [5] Y. T. Cheng, D. E. Rodak, C. A. Wong, C. A. Hayden, *Nanotechnology* **2006**, *17*, 1359.
- [6] H. J. Ensikat, P. Ditsche-Kuru, C. Neinhuis, W. Barthlott, *Beilstein J. Nanotechnol.* **2011**, *2*, 152.
- [7] B. Prüm, R. Seidel, H. F. Bohn, T. Speck, *J. R. Soc. Interface* **2012**, *9*, 127.
- [8] W. Barthlott, M. Mail, B. Bhushan, K. Koch, *Nano-Micro Lett.* **2017**, *9*, 23.
- [9] K. Koch, B. Bhushan, W. Barthlott, *Prog. Mater. Sci.* **2009**, *54*, 137.
- [10] B. Prüm, H. F. Bohn, R. Seidel, S. Rubach, T. Speck, *Acta Biomater.* **2013**, *9*, 6360.
- [11] B. Prüm, R. Seidel, H. F. Bohn, T. Speck, *Beilstein J. Nanotechnol.* **2012**, *3*, 57.
- [12] K. Koch, B. Bhushan, W. Barthlott, *Prog. Mater. Sci.* **2009**, *54*, 137.
- [13] A. del Campo, E. Arzt, *Chem. Rev.* **2008**, *108*, 911.
- [14] A. Carlson, A. M. Bowen, Y. Huang, R. G. Nuzzo, J. A. Rogers, *Adv. Mater.* **2012**, *24*, 5284.
- [15] Z. Nie, E. Kumacheva, *Nat. Mater.* **2008**, *7*, 277.
- [16] W.-G. Bae, H. N. Kim, D. Kim, S.-H. Park, H. E. Jeong, K.-Y. Suh, *Adv. Mater.* **2014**, *26*, 675.
- [17] W.-K. Lee, C. J. Engel, M. D. Huntington, J. Hu, T. W. Odom, *Nano Lett.* **2015**, *15*, 5624.
- [18] A. Bradley, J. P. Hammes, *J. Electrochem. Soc.* **1963**, *110*, 15.
- [19] H. K. Yasuda, *Plasma Polymerization*, Academic Press, San Diego, CA **2012**.
- [20] G. Nasti, S. Sanchez, I. Gunkel, S. Balog, B. Roose, B. D. Wilts, J. Teuscher, G. Gentile, P. Cerruti, V. Ambrogio, C. Carfagna, U. Steiner, A. Abate, *Soft Matter* **2017**, *13*, 1654.
- [21] E. Cerda, L. Mahadevan, *Phys. Rev. Lett.* **2003**, *90*, 074302.
- [22] J. Y. Chung, A. J. Nolte, C. M. Stafford, *Adv. Mater.* **2011**, *23*, 349.
- [23] H. E. Lindberg, *Little Book of Dynamic Buckling*, LCE Science/Software, Penn Valley CA **2003**.
- [24] J. Rodríguez-Hernández, *Prog. Polym. Sci.* **2015**, *42*, 1.
- [25] E. Gadelmawla, M. Koura, T. Maksoud, I. Elewa, H. Soliman, *J. Mater. Process. Technol.* **2002**, *123*, 133.
- [26] J. M. R. Bullock, W. Federle, *Insect Science* **2011**, *18*, 298.
- [27] D. Voigt, J. Schuppert, S. Dattinger, S. Gorb, *J. Insect Physiol.* **2008**, *54*, 765.
- [28] E. V. Gorb, N. Hosoda, C. Miksch, S. N. Gorb, *J. R. Soc. Interface* **2010**, *7*, 1571.
- [29] M. W. England, T. Sato, M. Yagihashi, A. Hozumi, S. N. Gorb, E. V. Gorb, *Beilstein J. Nanotechnol.* **2016**, *7*, 1471.
- [30] E. Gorb, S. Gorb, *Entomol. Exp. Appl.* **2009**, *130*, 222.
- [31] B. Prüm, H. F. Bohn, R. Seidel, S. Rubach, T. Speck, *Acta Biomater.* **2013**, *9*, 6360.
- [32] D. Chandra, A. J. Crosby, *Adv. Mater.* **2011**, *23*, 3441.
- [33] C. M. González-Henríquez, D. H. Sagredo-Oyarce, M. A. Sarabia-Vallejos, J. Rodríguez-Hernández, *Polymer* **2016**, *101*, 24.
- [34] J. Cong, J. Wang, J. Xie, C. Yang, J. Zhao, L. Li, Y. Cao, A. Fery, X.-Q. Feng, C. Lu, *Langmuir* **2018**, *34*, 4793.
- [35] M. Pretzl, A. Schweikart, C. Hanske, A. Chiche, U. Zettl, A. Horn, A. Böker, A. Fery, *Langmuir* **2008**, *24*, 12748.
- [36] B. Reid, M. Gibson, A. Singh, J. Taube, C. Furlong, M. Murcia, J. Elisseeff, *J. Tissue Eng. Regen. Med.* **2015**, *9*, 315.
- [37] E. Andrzejewska, *Prog. Polym. Sci.* **2001**, *26*, 605.
- [38] J. P. Mazzoccoli, D. L. Feke, H. Baskaran, P. N. Pintauro, *J. Biomed. Mater. Res., Part A* **2010**, *93A*, 558.
- [39] H. M. Azeredo, K. W. Waldron, *Trends Food Sci. Technol.* **2016**, *52*, 109.
- [40] H. Lei, L. F. Francis, W. W. Gerberich, L. E. Scriven, *AIChE J.* **2002**, *48*, 437.
- [41] S. K. Basu, L. Scriven, L. Francis, A. McCormick, *Prog. Org. Coat.* **2005**, *53*, 1.
- [42] J. Zhao, P. Yu, S. Dong, *Materials* **2016**, *9*, 4.
- [43] S. Gorb, *Attachment Devices of Insect Cuticle*, Springer Science & Business Media **2001**.
- [44] R. G. Beutel, S. Gorb, *J. Zoolog. Systemat. Evolut. Res.* **2001**, *39*, 177.
- [45] G. Kerstiens, *J. Exp. Bot.* **1996**, *47*, 50.
- [46] T. K. Sabu, K. Vinod, *J. Insect Sci.* **2009**, *9*, 72.
- [47] V. A. Surapaneni, G. Bold, T. Speck, M. Thielen, *bioRxiv* **2020**, <https://doi.org/10.1101/2020.04.14.040659>
- [48] D. Voigt, A. Schweikart, A. Fery, S. Gorb, *J. Exp. Biol.* **2012**, *215*, 1975.
- [49] D. Labonte, W. Federle, *Philos. Trans. R. Soc., B* **2015**, *370*, 1661.
- [50] J. M. Bullock, W. Federle, *Naturwissenschaften* **2011**, *98*, 381.